J. Meas. Sci. Instrum., 2023, 14(2): 218-225
DOI: 10.3969/j.issn.1674-8042.2023.02.011
http://xuebao.nuc.edu.cn
jmsi@nuc.edu.cn

Research on fixed time sliding mode control strategy based on RBF neural network

ZHANG Xin[1,2], QUAN Ying[1]

(1. *School of Automation & Electrical Engineering, Lanzhou Jiaotong University, Lanzhou 730070, China*;
2. *Gansu Provincial Engineering Research Center for Artificial Intelligence and Graphics & Image Processing, Lanzhou 730070, China*)

Abstract: In order to achieve high-precision tracking control of the end of manipulator, a fixed-time sliding mode tracking control strategy based on radial basis function (RBF) neural network is proposed. First, the dynamic model of the manipulator is established. Then the RBF neural network is combined with the fixed-time sliding mode surface to design the RBF fixed-time sliding mode controller to achieve high-precision control of the end trajectory of the manipulator. And the theoretical feasibility of the designed controller is proved by the Lyapunov stability theory. Finally, a simulation experiment is carried out with the two-joint manipulator as the research object. The results show that the fixed-time sliding mode tracking control strategy of the RBF neural network can estimate the uncertain parameters in the model, effectively improve the control effect, and make the controller have fixed-time convergence characteristics, which improves the convergence speed of the manipulator.

Key words: manipulator; radial basis function (RBF) neural network control; fixed-time sliding mode surface; Lyapunov function; convergence speed

0 Introduction

Manipulators can replace humans to perform some operational tasks with high risk factors, high speed and precision requirements, they have been widely used in many neighborhoods, such as industrial manufacturing[1], transportation[2], space exploration[3], agricultural production[4], medical and health[5] and other fields. The manipulator control system is a multi-input, multi-output, highly coupled, nonlinear and time-varying dynamic system. In practical applications, there will be parameter uncertainties and various external interferences. Therefore, it has important practical significance for the research on the effective position tracking control of the manipulator.

In view of the position tracking control problem of the manipulator, many control methods have been proposed, including sliding mode control[6-7], adaptive control[8], fuzzy control[9], neural network control[10] and so on. Sliding mode control is a special kind of nonlinear control. Its advantages are that it has strong robustness to uncertain parameters and external interference, and has simple structure and strong applicability[11]. Radial basis function (RBF) neural network has good nonlinear approximation ability, and it can achieve fast approximation speed without establishing an accurate model. However, in the entire control process, due to the existence of approximation errors, neural networks are often combined with other control methods to compensate for the effects of dynamic nonlinearity and various uncertainties, thereby improving the stability, convergence and robustness of the system[12].

In sliding mode control, when the state trajectory of the system reaches the sliding mode surface, although the ordinary linear sliding mode can be infinitely close to the equilibrium point, it cannot converge in a finite time. A new nonsingular integral terminal sliding mode control for robot manipulators is proposed, so that the state trajectory of the system can converge in a finite time[13]. A fractional-order non-singular terminal sliding mode control method is proposed, which achieves accurate tracking and finite

Received date: 2022-12-17

Foundation items: Natural Science Foundation of Gansu Province (No. 20JR5RA419); Lanzhou Jiaotong University-Tianjin University Innovation Fund Project (No. 2019053)

Corresponding author: QUAN Ying (q601477086@163.com)

time convergence of the cable manipulator[14]. A new adaptive neural network control strategy is proposed to solve the unknown weights of the radial basis function neural network (RBFNN) for unknown dynamics[15]. The advantages of terminal sliding mode control are combined with neural network control, and a new robust control scheme is proposed to achieve rapid convergence control of the robot[16]. However, none of the methods can make the state trajectory of the system converge within a fixed time range. The concept of fixed-time convergence is proposed[17]. Fixed-time control is essentially finite-time control. Its convergence time has nothing to do with the initial state conditions of the system, and there is an upper bound on the convergence time, but it is only studied for nonlinear systems. A new type of fixed-time sliding mode surface is designed[18] to make the tracking error of the manipulator converge quickly in a fixed time, without considering the influence of system uncertainty. A fixed-time terminal sliding mode controller is designed to solve the problem of accurate positioning of the ammunition transmission manipulator under the condition of basic vibration[19].

The RBF fixed-time sliding mode tracking control strategy is designed for the trajectory tracking control problem of the end effector of the manipulator with unmodeled dynamics and unknown external interference. The effectiveness and accuracy of the designed control system are verified by simulation experiments.

1 Dynamics model of manipulator

For then-joint rigid manipulator, according to the Lagrange equation, its dynamic model can be expressed as

$$\boldsymbol{M}(\boldsymbol{q})\ddot{\boldsymbol{q}}+\boldsymbol{C}(\boldsymbol{q},\dot{\boldsymbol{q}})\dot{\boldsymbol{q}}+\boldsymbol{G}(\boldsymbol{q})=\boldsymbol{\tau}, \tag{1}$$

where $\boldsymbol{q}\in\mathbf{R}^n$ is the joint position; $\dot{\boldsymbol{q}}\in\mathbf{R}^n$ and $\ddot{\boldsymbol{q}}\in\mathbf{R}^n$ are the velocity vector and acceleration vector; $\boldsymbol{M}(\boldsymbol{q})\in\mathbf{R}^{n\times n}$ is the inertia matrix; $\boldsymbol{C}(\boldsymbol{q},\dot{\boldsymbol{q}})\in\mathbf{R}^{n\times n}$ is the centrifugal force and Coriolis force matrix; $\boldsymbol{G}(\boldsymbol{q})\in\mathbf{R}^{n\times n}$ is the gravity term; $\boldsymbol{\tau}\in\mathbf{R}^n$ is the control moment.

In practical applications, due to the influence of external environmental noise and measurement errors, $\boldsymbol{M}(\boldsymbol{q})$, $\boldsymbol{C}(\boldsymbol{q},\dot{\boldsymbol{q}})$ and $\boldsymbol{G}(\boldsymbol{q})$ are not easy to be obtained. Considering the uncertainty of the parameters, they are divided into nominal values and disturbance values.

$$\boldsymbol{M}(\boldsymbol{q})=\boldsymbol{M}_0(\boldsymbol{q})+\Delta\boldsymbol{M}(\boldsymbol{q}), \tag{2}$$

$$\boldsymbol{C}(\boldsymbol{q},\dot{\boldsymbol{q}})=\boldsymbol{C}_0(\boldsymbol{q},\dot{\boldsymbol{q}})+\Delta\boldsymbol{C}(\boldsymbol{q},\dot{\boldsymbol{q}}), \tag{3}$$

$$\boldsymbol{G}(\boldsymbol{q})=\boldsymbol{G}_0(\boldsymbol{q})+\Delta\boldsymbol{G}(\boldsymbol{q}), \tag{4}$$

where $\boldsymbol{M}_0(\boldsymbol{q})$, $\boldsymbol{C}_0(\boldsymbol{q},\dot{\boldsymbol{q}})$ and $\boldsymbol{G}(\boldsymbol{q})$ are nominal values; $\Delta\boldsymbol{M}(\boldsymbol{q})$, $\Delta\boldsymbol{C}(\boldsymbol{q},\dot{\boldsymbol{q}})$ and $\Delta\boldsymbol{G}(\boldsymbol{q})$ are disturbance values.

Regarding system modeling errors, parameter changes and other uncertain factors as external disturbances, expressed by $\boldsymbol{\tau}_{\mathrm{d}}$, Eq. (1) can be expressed as

$$\boldsymbol{M}_0(\boldsymbol{q})\ddot{\boldsymbol{q}}+\boldsymbol{C}_0(\boldsymbol{q},\dot{\boldsymbol{q}})\dot{\boldsymbol{q}}+\boldsymbol{G}_0(\boldsymbol{q})=\boldsymbol{\tau}+\boldsymbol{\tau}_{\mathrm{d}}. \tag{5}$$

2 Design of RBF fixed time sliding mode controller

2.1 Design of fixed time sliding surface

According to the dynamic model of the manipulator, $\boldsymbol{q}_{\mathrm{d}}(t)$ is defined as the ideal position of the joint, and $\boldsymbol{q}(t)$ is the actual position of the joint. The position tracking error of each joint of the manipulator is defined as

$$\boldsymbol{e}(t)=\boldsymbol{q}_{\mathrm{d}}(t)-\boldsymbol{q}(t). \tag{6}$$

The second derivative of Eq. (6) is

$$\ddot{\boldsymbol{e}}=\ddot{\boldsymbol{q}}_{\mathrm{d}}-\ddot{\boldsymbol{q}}. \tag{7}$$

A type of fixed-time sliding surface is

$$\boldsymbol{s}=\dot{\boldsymbol{e}}+(\boldsymbol{a}\boldsymbol{e}^{\frac{p-q}{p}}+\boldsymbol{d})^2\boldsymbol{e}^{\frac{q}{p}}, \tag{8}$$

where $\boldsymbol{a}=\mathrm{diag}[a_1,a_2,\cdots,a_n]>0$; $\boldsymbol{d}=\mathrm{diag}[d_1,d_2,\cdots,d_n]>1$; p and q are both positive odd numbers, and $p>q$.

Lemma 1: In the fixed-time sliding mode surface (4), the time t_{s} for the system state to converge from the initial state $\boldsymbol{e}(0)$ to the equilibrium point $\boldsymbol{e}(t_{\mathrm{s}})$ has a fixed upper bound, and is not affected by the size of the initial state $\boldsymbol{e}(0)$[16].

Proof:

Item i in Eq. (8) is selected for analysis. When $\boldsymbol{s}=0$, Eq. (8) can be transformed into

$$e_i^{-\frac{q}{p}}\dot{e}_i+(a_ie_i^{\frac{p-q}{p}}+d_i)^2=0. \tag{9}$$

Let $w_i=e_i^{(p-q)/p}$, that is $e_i=w_i^{p/(p-q)}$, substituting Eq. (9) to get

$$\frac{p}{p-q}\dot{w}_i+(a_iw_i+d_i)^2=0. \tag{10}$$

The simplified Eq. (10) is

$$\dot{w}_i+\lambda_{1i}(w_i+\lambda_{2i})^2=0, \tag{11}$$

where $\lambda_{1i}=\dfrac{a_i^2(p-q)}{p}$; $\lambda_{2i}=\dfrac{d_i}{a_i}$.

Let $\dot{w}_i=\mathrm{d}w_i/\mathrm{d}t$, Eq. (11) can be expressed as

$$\mathrm{d}w_i=-\frac{1}{\lambda_{1i}(w_i+\lambda_{2i})^2}\mathrm{d}t. \tag{12}$$

Integrate both sides of Eq. (12) to get

$$t=\int_{w_i(t)}^{w_i(0)}\frac{1}{\lambda_{1i}(w_i+\lambda_{2i})^2}\mathrm{d}t=\frac{(w_i(0)+\lambda_{2i})^{-1}-(w_i(t)+\lambda_{2i})^{-1}}{-\lambda_{1i}}. \tag{13}$$

When the sliding mode state converges to the equilibrium point, e_i is infinitely close to 0, which is $w_i(t)=0$. It can be obtained that

$$t=\frac{\lambda_{2i}^{-1}}{\lambda_{1i}}-\frac{(w_i(0)+\lambda_{2i})^{-1}}{\lambda_{1i}}. \tag{14}$$

No matter how $w_i(0)$ changes, the convergence time t_s always has a fixed upper bound. So

$$t_s\leqslant t_{\max}=\frac{\lambda_{2i}^{-1}}{\lambda_{1i}}=\frac{p}{a_i(p-q)d_i}. \tag{15}$$

The characteristic of the fixed-time sliding surface is proved.

The derivative of Eq. (8) is

$$\dot{\boldsymbol{s}}=\ddot{\boldsymbol{e}}+\boldsymbol{H}, \tag{16}$$

where

$$\boldsymbol{H}=2\boldsymbol{a}\frac{p-q}{p}(\boldsymbol{a}\boldsymbol{e}^{\frac{p-q}{p}}+\boldsymbol{d})\dot{\boldsymbol{e}}+\frac{q}{p}(\boldsymbol{a}\boldsymbol{e}^{\frac{p-q}{p}}+\boldsymbol{d})^2\boldsymbol{e}^{\frac{q-p}{p}}\dot{\boldsymbol{e}}.$$

From Eqs. (5), (7) and (16), it can be obtained that

$$\dot{\boldsymbol{s}}=\boldsymbol{H}+\ddot{\boldsymbol{q}}_{\mathrm{d}}-\boldsymbol{M}_0^{-1}(\boldsymbol{\tau}+\boldsymbol{\tau}_{\mathrm{d}}-\boldsymbol{C}\dot{\boldsymbol{q}}-\boldsymbol{G}). \tag{17}$$

Select the exponential approach law as

$$\dot{\boldsymbol{s}}=-\boldsymbol{\lambda}\mathrm{sign}(\boldsymbol{s})-\boldsymbol{k}\boldsymbol{s}. \tag{18}$$

The combination of Eqs. (17) and (18) is simplified as

$$\boldsymbol{\tau}=\boldsymbol{M}_0(\boldsymbol{q})(\boldsymbol{H}+\boldsymbol{\lambda}\mathrm{sign}(\boldsymbol{s})+\boldsymbol{k}\boldsymbol{s})+\boldsymbol{f}(x)-\boldsymbol{\tau}_{\mathrm{d}}, \tag{19}$$

where $\boldsymbol{f}(x)=\boldsymbol{M}_0\ddot{\boldsymbol{q}}_{\mathrm{d}}+\boldsymbol{G}_0+\boldsymbol{C}_0\dot{\boldsymbol{q}}$.

Set the input of the neural network as

$$\boldsymbol{x}=[\boldsymbol{e}^{\mathrm{T}},\dot{\boldsymbol{e}}^{\mathrm{T}},\boldsymbol{q}_{\mathrm{d}}^{\mathrm{T}},\dot{\boldsymbol{q}}_{\mathrm{d}}^{\mathrm{T}},\ddot{\boldsymbol{q}}_{\mathrm{d}}^{\mathrm{T}}]. \tag{20}$$

2.2 RBFNN

Because RBFNN has good approximation characteristics, it can be used to compensate uncertain systems, thereby achieving more precise control. Define the RBF network function as

$$\varphi_i(x)=\exp\left(-\frac{\|x-c_i\|^2}{2b^2}\right),(i=1,2,\cdots n), \tag{21}$$

$$\boldsymbol{f}(x)=\boldsymbol{W}^{\mathrm{T}}\boldsymbol{\varphi}(x)+\boldsymbol{\mu}, \tag{22}$$

where x is the input signal of the neural network; $\boldsymbol{W}$ is the weight vector of the neural network; $\boldsymbol{\varphi}(x)$ is the output vector of the intermediate layer of the neural network; $\boldsymbol{\mu}$ is the approximation error of the neural network; c_i is the central value vector of the i-th interneuron of the RBF neural network; b is the width value of the interneuron.

The output $\hat{\boldsymbol{f}}(x)$ of the RBF network is the estimated value of $\boldsymbol{f}(x)$.

$$\hat{\boldsymbol{f}}(x)=\hat{\boldsymbol{W}}^{\mathrm{T}}\boldsymbol{\varphi}(x). \tag{23}$$

Define the error term $\tilde{\boldsymbol{f}}(x)=\boldsymbol{f}(x)-\hat{\boldsymbol{f}}(x)$, then

$$\tilde{\boldsymbol{f}}(x)=\tilde{\boldsymbol{W}}^{\mathrm{T}}\boldsymbol{\varphi}(x)+\boldsymbol{\mu}, \tag{24}$$

where $\tilde{\boldsymbol{W}}=\boldsymbol{W}-\hat{\boldsymbol{W}}$. $\tilde{\boldsymbol{W}}$, $\boldsymbol{W}$ and $\hat{\boldsymbol{W}}$ are the error value, actual value and approximate value of the network weight, respectively.

The combination of Eqs. (19) and (23) is simplified as

$$\boldsymbol{\tau}=\boldsymbol{M}_0(\boldsymbol{q})(\boldsymbol{H}+\boldsymbol{\lambda}\mathrm{sign}(\boldsymbol{s})+\boldsymbol{k}\boldsymbol{s})+\hat{\boldsymbol{W}}^{\mathrm{T}}\boldsymbol{\varphi}(x)-\boldsymbol{\tau}_{\mathrm{d}}-\boldsymbol{r}, \tag{25}$$

where $\boldsymbol{r}=-\boldsymbol{\mu}_{\mathrm{N}}\mathrm{sign}(\boldsymbol{s})$ is a robust term that overcomes the estimation error of the neural network.

Design the RBF network weight adaptive law as

$$\dot{\hat{\boldsymbol{W}}}=\boldsymbol{\Gamma}\boldsymbol{M}_0^{-1}\boldsymbol{\varphi}(x)\boldsymbol{s}^{\mathrm{T}}, \tag{26}$$

where $\boldsymbol{\Gamma}=\boldsymbol{\Gamma}^{\mathrm{T}}>0$.

2.3 Stability analysis

The Lyapunov function is selected, that is

$$V=\frac{1}{2}\boldsymbol{s}^{\mathrm{T}}\boldsymbol{s}+\frac{1}{2}\mathrm{tr}(\tilde{\boldsymbol{W}}^{\mathrm{T}}\boldsymbol{\Gamma}^{-1}\tilde{\boldsymbol{W}}). \tag{27}$$

Eq. (27) is a positive definite function, and the two sides are derived as

$$\dot{V}=\boldsymbol{s}^{\mathrm{T}}\dot{\boldsymbol{s}}+\tilde{\boldsymbol{W}}^{\mathrm{T}}\boldsymbol{\Gamma}^{-1}\dot{\tilde{\boldsymbol{W}}}. \tag{28}$$

From $\tilde{\boldsymbol{W}}=\boldsymbol{W}-\hat{\boldsymbol{W}}$ to know $\dot{\tilde{\boldsymbol{W}}}=-\dot{\hat{\boldsymbol{W}}}$, substituting Eqs. (17) and (25) into Eq. (28), it can be obtained that

$$\dot{V}=\boldsymbol{s}^{\mathrm{T}}(-\boldsymbol{\lambda}\operatorname{sign}(\boldsymbol{s})-\boldsymbol{k}\boldsymbol{s}-\boldsymbol{M}_0^{-1}\tilde{\boldsymbol{W}}^{\mathrm{T}}\boldsymbol{\varphi}(x))-\tilde{\boldsymbol{W}}^{\mathrm{T}}\boldsymbol{\Gamma}^{-1}\dot{\hat{\boldsymbol{W}}}=$$

$$\boldsymbol{s}^{\mathrm{T}}(-\boldsymbol{\lambda}\operatorname{sign}(\boldsymbol{s})-\boldsymbol{k}\boldsymbol{s})-\tilde{\boldsymbol{W}}^{\mathrm{T}}(\boldsymbol{s}^{\mathrm{T}}\boldsymbol{M}_0^{-1}\boldsymbol{\varphi}(x)-\boldsymbol{\Gamma}^{-1}\dot{\hat{\boldsymbol{W}}})=$$

$$\boldsymbol{s}^{\mathrm{T}}(-\boldsymbol{\lambda}\operatorname{sign}(\boldsymbol{s})-\boldsymbol{k}\boldsymbol{s})-\tilde{\boldsymbol{W}}^{\mathrm{T}}(\boldsymbol{s}^{\mathrm{T}}\boldsymbol{M}_0^{-1}\boldsymbol{\varphi}(x)-\boldsymbol{\Gamma}^{-1}\dot{\hat{\boldsymbol{W}}})\leqslant 0. \tag{29}$$

According to the Lyapunov stability criterion, the system can be judged to be asymptotically stable.

3 Simulation results

The two-joint robotic arm is taken as an example for simulation verification. According to the dynamic model of the robotic arm system in the previous article, its specific parameters are

$$\boldsymbol{M}(\boldsymbol{q})=\begin{bmatrix} v+q_{01}+2q_{02}\cos q_2 & q_{01}+q_{02}\cos q_2 \\ q_{01}+q_{02}\cos q_2 & q_{01}\end{bmatrix},$$

$$\boldsymbol{C}(\boldsymbol{q},\dot{\boldsymbol{q}})=\begin{bmatrix} -q_{02}\dot{q}_2\sin q_2 & -q_{02}(\dot{q}_1+\dot{q}_2)\sin q_2 \\ q_{02}\dot{q}_1\sin q_2 & 0\end{bmatrix},$$

$$\boldsymbol{G}(\boldsymbol{q})=\begin{bmatrix} 15g\cos q_1+8.75g\cos(q_1+q_2) \\ 8.75g\cos(q_1+q_2)\end{bmatrix},$$

$$\boldsymbol{\tau}_{\mathrm{d}}=10\sin(2\pi t),$$

where $v=13.33$; $q_{01}=8.98$; $q_{02}=8.75$; $g=9.8$. The two joint position commands are $q_{1\mathrm{d}}=\cos(\pi t)$, $q_{2\mathrm{d}}=\sin(\pi t)$. The initial state of the two-joint manipulator system is given as $[q_1 \quad q_2 \quad q_3 \quad q_4]=[0.6 \quad 0.3 \quad -0.5 \quad 0.5]$, and $\boldsymbol{\lambda}=\operatorname{diag}[0.5,0.5]$, $\boldsymbol{k}=\operatorname{diag}[40,40]$.

The following control methods 1－5 are used to compare and analysis the simulation results.

Method 1: Fixed-time sliding mode control.

$$\boldsymbol{s}=\dot{\boldsymbol{e}}+(a\boldsymbol{e}^{\frac{p-q}{p}}+\boldsymbol{d})^2\boldsymbol{e}^{\frac{q}{p}}. \tag{30}$$

Method 2: Fast terminal sliding mode control.

$$\boldsymbol{s}=\dot{\boldsymbol{e}}+a\boldsymbol{e}+\boldsymbol{d}\boldsymbol{e}^{\frac{q}{p}}. \tag{31}$$

Method 3: Traditional sliding mode control.

$$\boldsymbol{s}=c\boldsymbol{e}+\dot{\boldsymbol{e}}. \tag{32}$$

Method 4: RBF fixed-time sliding mode control.

$$\boldsymbol{\tau}=\boldsymbol{M}_0(\boldsymbol{q})(\boldsymbol{H}+\boldsymbol{\lambda}\operatorname{sign}(\boldsymbol{s})+\boldsymbol{k}\boldsymbol{s})+\hat{\boldsymbol{W}}^{\mathrm{T}}\boldsymbol{\varphi}(x)-\boldsymbol{\tau}_{\mathrm{d}}-\boldsymbol{r}. \tag{33}$$

Method 5: PD type iterative learning control[20].

$$\boldsymbol{u}_{k+1}(t)=\boldsymbol{u}_k(t)+\boldsymbol{K}_{\mathrm{d}}\dot{\boldsymbol{e}}+\boldsymbol{K}_{\mathrm{p}}\boldsymbol{e}, \tag{34}$$

where $\boldsymbol{a}=\operatorname{diag}[1,1]$; $\boldsymbol{b}=\operatorname{diag}[2,2]$; $\boldsymbol{c}=\operatorname{diag}[2,2]$; $\boldsymbol{K}_p=[100 \quad 0;0 \quad 100]$; $\boldsymbol{K}_{\mathrm{d}}=[300 \quad 0;0 \quad 300]$.

Without interference, methods 1－3 are compared. Fig. 1 shows the position tracking of the three control methods. All three methods can achieve relatively effective tracking. Through comparative analysis, it can be seen that fixed-time sliding mode control has better tracking effect than fast terminal sliding mode control and sliding mode control, and its tracking performance is better.

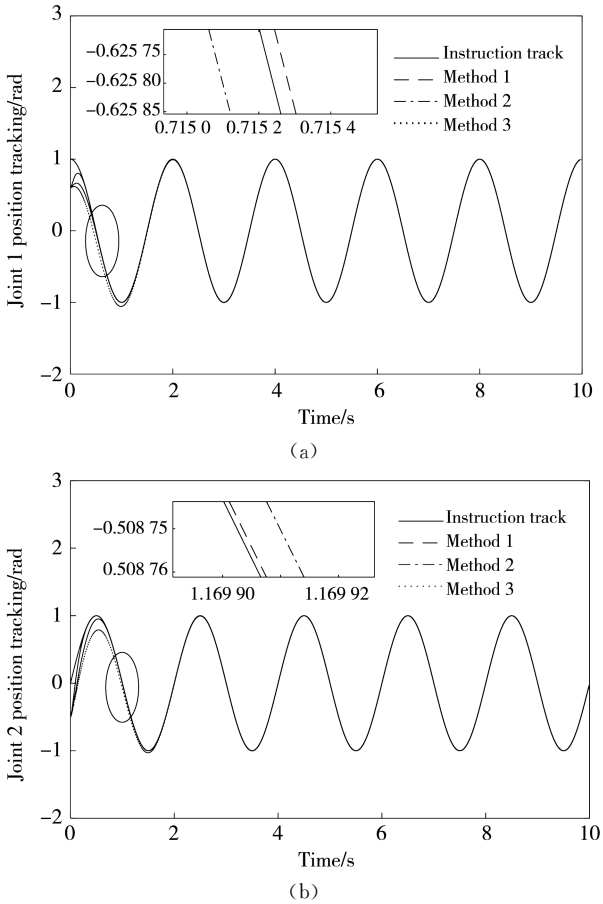

Fig. 1 Position tracking of joint 1 (a) and joint 2 (b)

Fig. 2 shows the comparison of the position error convergence of the robot arm of the three methods. It can be seen that the error convergence speed of method 1 is faster than that of other methods.

Fig. 3 shows the comparison of the speed error convergence of the robot arm of the three methods. By comparing the root mean square error of the three methods, it can be seen that the speed error convergence effect of method 1 is better than that of other methods.

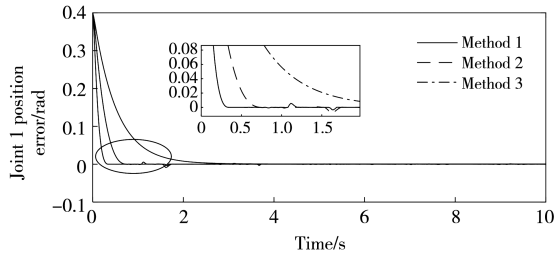

(a)

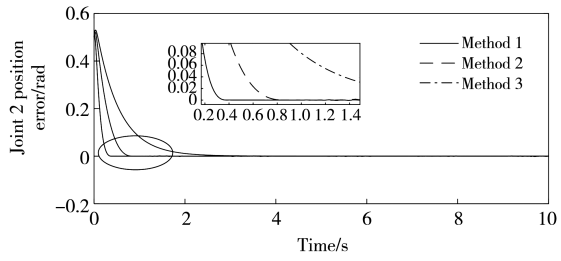

(b)

Fig. 2 Convergence of position error of joint 1 (a) and joint 2 (b)

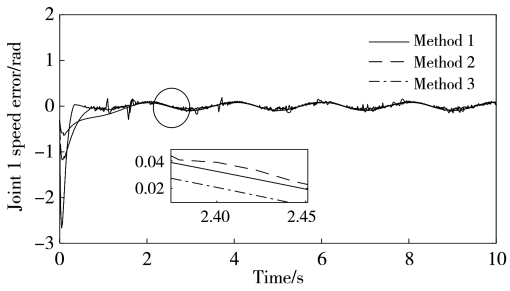

(a)

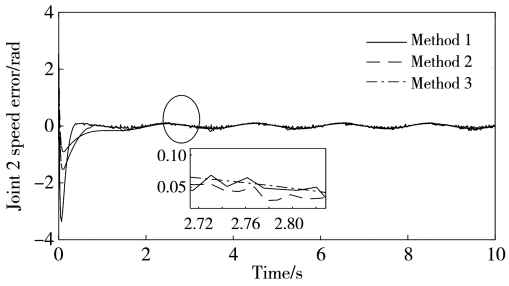

(b)

Fig. 3 Convergence of speed error of joint 1 (a) and joint 2 (b)

In order to analyze the performance of the control method more clearly, the root mean square error of the angular displacement adjustment time, position error and speed error are selected as the judgment reference value. Angular displacement adjustment time refers to the time that it takes for the angular displacement to change from the initial state to the tracking error less than or equal to 0.01 rad. The root mean square error can reflect the deviation between the observed value and the true value to realize the judgment of the following performance. Table 1 is obtained according to the simulation data analysis. It can be found that the performance of fixed-time sliding mode control is better than fast terminal sliding mode control and traditional sliding mode control.

Table 1 Comparison of method 1, method 2 and method 3

Performance	Method 1	Method 2	Method 3
Joint 1 angular displacement adjustment time/s	0.26	0.56	1.90
Joint 2 angular displacement adjustment time/s	0.30	0.68	2.08
Root mean square error of joint 1 position error after 2.5 s/rad	2.37×10^{-4}	2.61×10^{-4}	4.64×10^{-4}
Root mean square error of joint 2 position error after 2.5 s/rad	1.99×10^{-4}	3.14×10^{-4}	6.70×10^{-4}
Root mean square error of joint 1 speed error after 2.5 s/rad	4.92×10^{-2}	6.50×10^{-2}	6.55×10^{-2}
Root mean square error of joint 2 speed error after 2.5 s/rad	4.95×10^{-2}	6.81×10^{-2}	6.50×10^{-2}

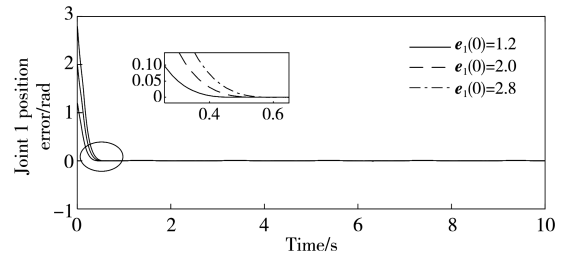

(a)

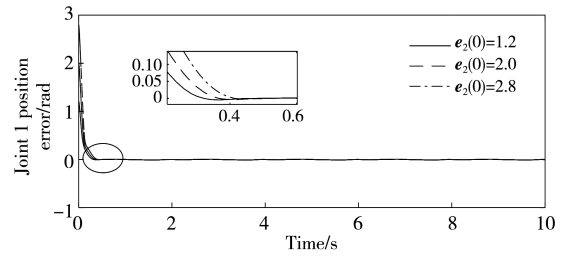

(b)

Fig. 4 Convergence effect of position tracking error of joint 1 (a) and joint 2 (b)

For method 4, take the absolute values of the initial errors of the trajectory of the robotic arm joint 1 and joint 2 respectively as $\boldsymbol{e}(0)=1.2$ rad, $\boldsymbol{e}(0)=2$ rad and $\boldsymbol{e}(0)=2.8$ rad. Fig. 4 shows the trajectory tracking of the robotic arm joint 1 and joint 2. It can be seen that regardless of the initial trajectory error of the manipulator joint, the convergence time of the joint position tracking error is the same and less than the theoretical upper limit of convergence time t_s, which reflects its fixed-time convergence characteristics.

With interference, method 4 and method 5 are compared, and the initial state is $[q_1 \quad q_2 \quad q_3 \quad q_4]=[0.5 \quad 0 \quad -0.5 \quad 0]$. The position tracking situation of the two control methods 4 and 5 is shown in Fig. 5. It can be seen that the two methods can achieve effective tracking of

the manipulator in the later stage, and the tracking effect of the RBF fixed-time sliding mode control is better than that of the PD-type iterative learning control.

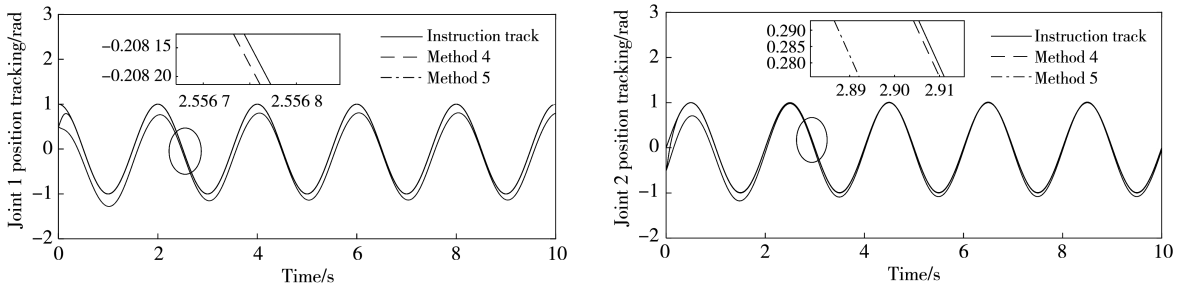

(a) (b)

Fig. 5 Position tracking of joint 1 (a) and joint 2 (b)

Fig. 6 shows the comparison results of the position error convergence of the manipulators between method 4 and method 5. It shows that the position error convergence effect of method 4 is significantly better than that of method 5. Method 5 has a faster convergence rate.

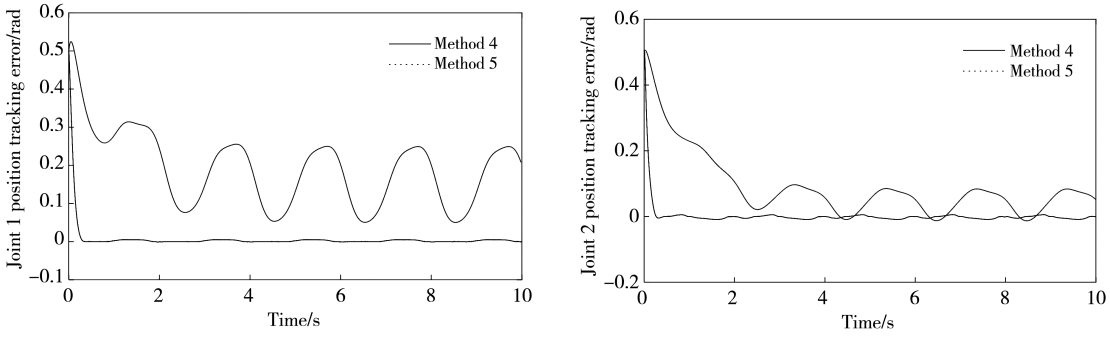

(a) (b)

Fig. 6 Convergence of position error of joint 1 (a) and joint 2 (b)

Fig. 7 shows the comparison results of the speed error convergence of the manipulators of method 4 and method 5. By comparing the root mean square error, it can be seen that the speed error convergence effect of method 4 is significantly better than that of method 5.

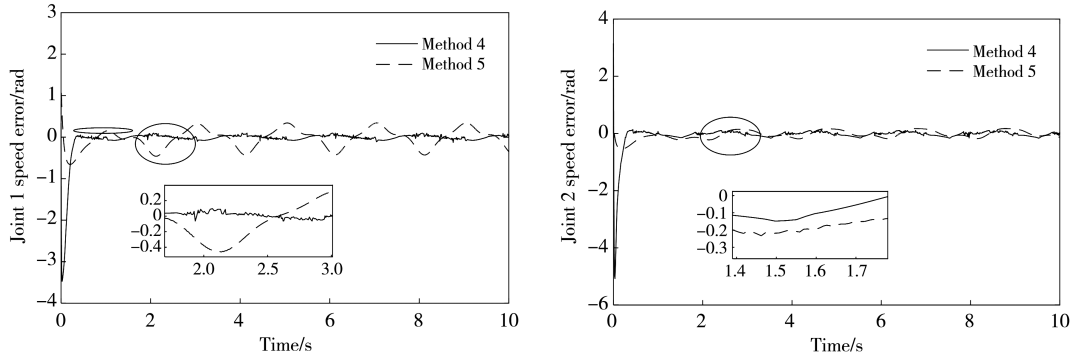

(a) (b)

Fig. 7 Convergence of speed error of joint 1 (a) and joint 2 (b)

In order to analyze the performance of the control method more clearly, the simulation data of method 4 and method 5 are showed in Table 2. It can be found that the performance of RBF fixed-time sliding mode control is better than that of PD-type iterative learning control.

Table 2 Comparison results of method 4 and method 5

Performance	Method 4	Method 5
Root mean square error of joint 1 position error after 2 s/rad	1.81×10^{-3}	6.78×10^{-2}
Root mean square error of joint 2 position error after 2 s/rad	3.74×10^{-3}	6.79×10^{-2}
Root mean square error of joint 1 speed error after 2 s/rad	4.03×10^{-2}	6.07×10^{-2}
Root mean square error of joint 2 speed error after 2 s/rad	5.76×10^{-2}	6.59×10^{-2}

4 Conclusions

In order to improve the control accuracy of the robot arm end effector trajectory with unmodeled dynamics and unknown external disturbances, an RBF fixed-time sliding mode tracking control strategy is designed based on the dynamic model of the robot arm. Through simulation and comparison with PD-type iterative learning control, these conclusions are obtained.

1) The method proposed in this paper has fixed time convergence characteristics. The initial trajectory error of different manipulator joints is set, and the convergence time of the joint position tracking error is the same and less than the upper limit of the theoretical convergence time.

2) Compared with PD-type iterative learning control, the proposed method has better tracking performance. It improves the control accuracy and convergence speed to a certain extent, so that the root mean square error of the position error and velocity error of the two manipulator joints are reduced. The root mean square error of the position error is reduced by 6.699×10^{-2} rad and 6.416×10^{-2} rad. And the root mean square error of velocity error is reduced by 2.04×10^{-2} rad and 8.3×10^{-3} rad.

References

[1] KANGRU T, RIIVES J, MAHMOOD K, et al. Suitability analysis of using industrial robots in manufacturing. Proceedings of the Estonian Academy of Sciences, 2019, 68(4): 383-388.

[2] HUA Y, GU Y X. Kinematics analysis of a robotic arm in a traffic cone automatic recovery and placement device. Mechanical Engineering and Technology, 2020, 9(1): 1-12.

[3] HIRZINGER G, BRUNNER B, LANDZETTEL K, et al. Space robotics-DLR's telerobotic concepts, lightweight arms and articulated hands. Autonomous Robots, 2003, 14(2): 127-145.

[4] ARAD B, BALENDONCK J, BARTH R, et al. Development of a sweet pepper harvesting robot. Journal of Field Robotics, 2020, 37(6): 1027-1039.

[5] SUN P, WANG S Y, KARIMI H R, et al. Robust redundant input reliable tracking control for omnidirectional rehabilitative training walker. Mathematical Problems in Engineering, 2014, 2014(Pt. 2): 636934.

[6] SOUHILA A B, FETHI D, ABDELHAFID O. Design of a sliding mode observer based on computed torque control for hyper dynamic manipulation. Journal Européen des Systèmes Automatisés, 2019, 52(5): 449-456.

[7] MIAO Z C, ZHANG W B, HANT L, et al. Fractional order integral sliding mode control for PMSM based on fractional order sliding mode observer. Journal of Measurement Science and Instrumentation, 2019, 10(4): 389-397.

[8] WANG D, HE H B, LIU D R. Adaptive critic nonlinear robust control: A survey. IEEE Transactions on Cybernetics, 2017, 47(10): 3429-3451.

[9] WANG M, BIAN G R, LI H S. A new fuzzy iterative learning control algorithm for single joint manipulator. Archives of Control Sciences, 2016, 26(3): 297-310.

[10] XU Y Y, WANG Y, XUE D B. Neural network control optimization and simulation of robot arm. Chinese Journal of Construction Machinery, 2018, 16(5): 416-420.

[11] ZHANG H, DONG H Y, ZHANG B P, et al. Research on beam supply control strategy based on sliding mode control. Archives of Electrical Engineering, 2020, 69(2): 349-364.

[12] SHI X P, LIU S R. Research progress of manipulator trajectory tracking control. Control Engineering, 2011, 18(1): 116-122+132.

[13] SU Y X, ZHENG C H. A new nonsingular integral terminal sliding mode control for robot manipulators. International Journal of Systems Science, 2020, 51(8): 1418-1428.

[14] WANG Y Y, JIANG S R, CHEN B, et al. A new continuous fractional-order nonsingular terminal sliding mode control for cable-driven manipulators. Advances in Engineering Software, 2018, 119: 21-29.

[15] LUAN F J, NA J, HUANG Y B, et al. Adaptive neural network control for robotic manipulators with guaranteed finite-time convergence. Neurocomputing, 2019, 337: 153-164.

[16] RUCHIK A, KUMAR N. Finite time control scheme for robot manipulators using fast terminal sliding mode control and RBFNN. International Journal of Dynamics and Control, 2019, 7(2): 758-766.

[17] POLYAKOV A. Nonlinear feedback design for fixed-time stabilization of linear control systems. IEEE Transactions on Automatic Control, 2012, 57(8): 2106-2110.

[18] WU D H, XIAO R, OUYANG H C, et al. Improved fixed-time sliding mode control method design of mechanical arm. Mechanical Science and Technology, 2021, 40(8): 1171-1176.

[19] YAO L P, HOU B L. Fixed-time terminal sliding mode control of ammunition transmission manipulator. Journal of Harbin Institute of Technology, 2021, 53(1): 109-116.

[20] LIU J K. Design of robot control system and MATLAB simulation. Beijing: Tsinghua University Press, 2008.

基于 RBF 神经网络的固定时间滑模控制策略研究

张 鑫[1,2], 权 莹[1]

(1. 兰州交通大学 自动化与电气工程学院, 甘肃 兰州 730070;
2. 甘肃省人工智能与图形图像处理工程研究中心, 甘肃 兰州 730070)

摘 要: 为了实现对机械臂末端的高精度跟踪控制, 本文提出了一种基于径向基函数(Radial basis function, RBF)神经网络的固定时间滑模跟踪控制策略。首先, 建立机械臂的动力学模型。然后, 将 RBF 神经网络和固定时间滑模面结合, 设计 RBF 固定时间滑模控制器, 以实现对机械臂末端轨迹的高精度控制; 并利用 Lyapunov 稳定性理论对所设计控制器的理论可行性进行了证明。最后, 以二关节机械臂为研究对象进行仿真实验。结果表明: RBF 神经网络的固定时间滑模跟踪控制策略能估计模型中的不确定参数, 有效地改善了控制效果; 并使控制器具有固定时间收敛特性, 提高了机械臂的收敛速度。

关键词: 机械臂; 径向基函数神经网络控制; 固定时间滑模面; Lyapunov 函数; 收敛速度

引用格式: ZHANG Xin, QUAN Ying. Research on fixed time sliding mode control strategy based on RBF neural network. Journal of Measurement Science and Instrumentation, 2023, 14(2): 218-225. DOI: 10.3969/j.issn.1674-8042.2023.02.011